Research Article

Acid mine drainage pollution remediation using hybrid chelating ion-exchange/$HZrO_2$ nanocomposite adsorbents

Caroline Lomalungelo Dlamini[1] · Lueta-Ann De Kock[1] · Kebede Keterew Kefeni[1] · Bhekie Brilliance Mamba[1] · Titus Alfred Makudali Msagati[1]

Received: 13 July 2019 / Accepted: 26 October 2019 / Published online: 16 November 2019

Abstract
Environmental pollution due to acid mine drainage (AMD) is a worldwide concern because of its high content of toxic metals and acidity. The toxic metal species present in AMD tends to affect negatively the whole ecological system where it is discharged, and this requires an elective solution to remedy the environment. In this study, hydrated ZrO_2 nanoparticles (HZO) were irreversibly dispersed within chelating ion-exchange resins using the precipitation method, resulting in HZO-260, HZO-207, HZO-214, HZO-4195 and HZO-900 organic/inorganic nanosorbents which were used for the removal of metals from AMD. The synthesized nanosorbents were characterized using SEM–EDS, FTIR and XRD. The effect of time, adsorbent dosage and pH on Al(III) adsorption was investigated using the batch technique. The SEM–EDS confirmed the incorporation of HZO within all the parent resins, while XRD showed that the hybrid materials were amorphous. The adsorption of Al(III) occurred through physisorption and was favourable only onto HZO-260 as revealed by the data modelling. Metal levels were determined using the ICP-OES technique. The HZO-260 removed 100% Al(III) in acidic conditions and was successfully regenerated for reuse using a NaCl–NaOH binary solution (pH > 12). HZO-260 removed selected metals (Al, Cr, Mn, Fe, Ni, Co, Cu, Zn, Pb and Cd) from environmental AMD. Therefore, HZO-260 has a promising potential as an adsorbent for AMD remediation.

Keywords Adsorption · Metal removal · Organic/inorganic nanosorbents · Zirconium oxide nanoparticle

1 Introduction

Mining is one of the important economic sectors that form the economic backbone of most countries worldwide [3, 21, 40]. The minerals of interest usually occur in nature with metal sulphide rocks such as iron sulphide (pyrite) in their strata, and pyrites are of paramount concern to environmentalists because upon exposure to the atmosphere, they quickly react with water and air to produce acidic effluents known as acid mine drainage (AMD) [4, 16]. AMD is characterized by high concentrations of H^+, Fe^{2+} and SO_4^{2-} species. Once AMD is formed, either in the mine voids or in the stockpiles of waste rock, it eventually finds its way through percolation, seepage, leachate, run-offs or even decanting to pollute water sources, thus rendering the water acidic [16]. When acidic water is in contact with different geologic materials such as mineral rocks, then toxic metals can be easily leached out and the solution gets laden with metal ions [18]. Generally, AMD acts as a vehicle for toxic metal pollution in the environment and the same toxic metals are a known recalcitrant bio-accumulative systemic toxins which cause carcinogenic, mutagenic, teratogenic, fetotoxic, neurotoxic and nephrotoxic effects to humans [22]. Moreover, the acidic metal-laden water upsets the whole ecological system as AMD-polluted water is always devoid of life [28]. The water habitat

✉ Titus Alfred Makudali Msagati, msagatam@unisa.ac.za | [1]College of Science Engineering and Technology, Nanotechnology and Water Sustainability Research Unit, University of South Africa, The Science Campus, Johannesburg, South Africa.

and aesthetic values are destroyed by AMD pollution. The worst part is that once AMD is produced, it persists for centuries, thus polluting the environment endlessly [9].

AMD is so disastrous to the environment such that in the year 1987 the United States Environmental Protection Agency (USEPA) declared it second only to global warming and stratospheric ozone depletion in ecological risk [16, 29]. Since then, treatment technologies have been sought worldwide to remediate toxic metal pollution in the environment. Unfortunately, traditional AMD treatment technologies use chemicals that produce wastes that are hazardous to the environment [25]. Therefore, there is a need for green technologies to be explored to save the environment from toxic metal (AMD) pollution.

One of the attractive technologies to effectively address AMD pollution to the environment involves adsorption process. These processes are an attractive technology for toxic metal removal from solutions, due to the fact that they employ adsorbents with high surface area-to-volume ratio, thus only small amounts are required, and the waste generated may not lead to secondary pollution. Moreover, the loaded adsorbents may also be amenable to regeneration for multiple reuse and recovery of the pollutants as valuable products. Thus, adsorption processes are cheap, simple and environmentally friendly [38]. Metal oxides are renowned metal scavengers in the environment and are a good choice of adsorbents for dissolved metals [10, 14, 17]. Therefore, since metal oxides have a special affinity for dissolved metals in the environment, they can be carefully engineered for the efficient removal of the same from solutions. Their adsorptive properties are enhanced when they are in the nanoscale [46]. Advantages of metal oxide nanoparticles (MONPs) as adsorbents include high adsorption efficiency, fast kinetics, amphoteric surfaces in addition to the fact that their synthesis involves procedures that are safe, simple and cost-effective [41]. Unfortunately, MONPs suffer from aggregation and weak mechanical strength to withstand flow-through systems for application purposes [45]. To overcome this limitation, researchers have dispersed MONPs into various polymeric materials for support-producing hybrid composite adsorbents with multiple advantageous properties [34, 39, 44].

Zirconium (IV) oxide is one of the polyvalent metal oxides that can remove both organic and inorganic pollutants from water. Zirconium oxide has the advantage of high chemical stability [32] and is rich in surface hydroxyl groups [20], which make it attractive for use as an adsorbent for metals from highly acidic solutions like AMD. According to the literature, the use of organic-supported hydrated Zr(IV) oxide nanocomposites has been reported for the removal of metals from wastewaters. Cho and co-workers prepared a ZrO_2/chitosan beads adsorbent (HZOCBs) for the removal of F^- and Pb^{2+} from solution [8]. HZOCBs exhibited efficient and rapid removal of Pb(II) ions with a maximum adsorption capacity of 222.2 mg/g. The adsorption of Pb(II) on the hybrid material occurred in a single-layer fashion. In another study, Pan and others fabricated a porous anion exchanger-supported hydrous Zr oxide adsorbent (HZO-201) and used it for the removal of As from groundwater and acidic mine water [32]. HZO-201 demonstrated a superior removal of As from the waters as compared to the Fe oxide-laden hybrid with the same host (HFO-201). The hybrid resin was amenable to regeneration for reuse using NaOH-NaCl binary solution with negligible loss in adsorption capacity. Padungthon and co-workers also synthesized a hybrid anion-exchange resin impregnated with ZrO_2 nanoparticles (HAIX-Zr) for the removal of both As(III) and As(V) ions from water [31]. The hybrid resin selectively removed both As species in the background of high concentration of competing ions. Similar to the previous study, they found that HAIX-Zr can be efficiently (> 90%) regenerated for reuse using the binary solution. They concluded that the hybrid adsorbent is very stable, it can immobilize the adsorbed As forever, and finally, the exhausted As-loaded nanosorbents can be safely disposed of in a landfill without the As leaching off into the environment.

In this study, the chemically stable Zr(IV) oxide was dispersed within various chelating resins for support-producing hybrid chelating ion-exchange resins (HLIX) for the removal of metals from the hostile AMD. Chelating resins exhibit better removal of metal ions over cation and anion-exchange resins. Thus, they are a good choice of support material for MONPs for metal pollution remediation. To the best of our knowledge, chelating resin-supported hydrated zirconium oxide nanosorbents for metal pollution remediation in acidic industrial wastewaters including AMD were for the first time produced and reported by this study. The major constituents of the Wits gold mines' AMD in South Africa are Al(III), Fe(II) and Mn(II) [18, 24]. Of the metals, Al(III) has received less attention from researchers, yet it is as much toxic as the so-called heavy metals [22, 30, 46]. Secondly, Al(III) is the most sensitive to high conductivity and low pH conditions, which are both characteristic of AMD, where it readily leaches from geologic material to contaminate water resources [7]. Hence in this study, Al(III) was used to investigate the adsorption efficiency of the synthesized HLIX. In humans, Al can affect both hard and soft tissues leading to detrimental health effects. Aluminium poisoning causes bone disease, *osteomalacia*; the Al(III) ions compete and exchange sites with the Ca^{2+} in the bones. When Al affects the nervous system, it causes *Alzheimer's disease* and in cells it compromises the immune system [6]. Aluminium is also carcinogenic. In aquatic life, Al(III) smothers the gills disturbing the enzymes responsible for uptake of ions leading to death [35]. In soils Al

inhibits the nutrient uptake by the plant roots [37] leading to dwarfism or even death of the plants. This may compromise food security and may result in deforestation. Aluminium in AMD impacted water (pH < 4.5) exists as an Al-SO_4^+ complex and as the most toxic free ion, Al^{3+}. Both species increase with the decrease in pH of the polluted water [36].

Therefore, the objectives of this study were to impregnate hydrated Zr oxide nanoparticles into different macroporous polystyrene-based chelating resins producing hybrid HZO nanocomposites for the adsorption of metal ions from solutions, to characterize the fabricated hybrid nanocomposite materials and finally to use them for the removal of metal ions from environmental AMD.

2 Experimental procedures

2.1 Preamble

In this work, hybrid ion-exchange Zr(IV) oxide adsorbents were synthesized by precipitation followed by mild thermal treatment and then characterized using a range of techniques to evaluate the success of the synthesis. Batch adsorption studies to evaluate the adsorbents' performance and the mechanisms of the adsorption were carried out using synthetic solutions composed of the major AMD components: Al(III), Fe(II), Mn(II) and SO_4^{2-}. This was followed by the desorption of the metals from the loaded resins. Finally, the adsorbents were tested on environmental AMD samples obtained from a defunct gold mine located in the western part of Gauteng Province, South Africa, for the removal of 10 selected metals, namely Al, Cr, Mn, Fe, Ni, Co, Cu, Zn, Pb and Cd.

2.2 Synthesis of hybrid Zr(IV) oxide adsorbents

All chemicals used in the experiments were of analytical grade purchased from Sigma-Aldrich (Johannesburg, South Africa). Five different macroporous polystyrene cross-linked divinyl benzene (DVB) resins were used as host materials for Zr(IV) oxide nanoparticles producing hybrid HZO adsorbents to study their efficiency on metal ions adsorption. Three of these host resins (alkylaminophosphonate, iminodiacetate and thiourea) were of the weakly acidic chelating type, while the other two were anionic (a weakly basic chelating bis-picolylamine and a strongly basic quaternary ammonium types) producing HZO-260, HZO-207, HZO-214, HZO-4195 and HZO-900 nanocomposites, respectively. The host resins were washed by shaking 50 g of each with 250 mL DI water in a prewashed 500-mL conical flask using an orbital shaker set at a speed of 150 rpm for 2 h. This procedure was carried out 3 times with fresh DI water each time. A 0.1 M solution of 99.99% zirconium (IV) sulphate hydrate was prepared using deionized water and was used to load the Zr(IV) ions into the L260 host resin. All the other host resins were loaded using 1 M solution of zirconium oxychloride ($ZrOCl_2{\cdot}8H_2O$). Metal loading solutions for anion exchangers were prepared by dissolving the metal salt ($ZrOCl_2{\cdot}8H_2O$) in 1 M dilute HCl in an ice bath [33]. The full synthesis procedure for the hybrid nanosorbents was done in three steps. The first step was the loading of the Zr ions into the 50 g washed resin by shaking with 250 mL loading solution in an orbital shaker set at 150 rpm in room temperature for 24 h. The supernatant was decanted and discarded appropriately. The next step was the simultaneous desorption and precipitation of the zirconium ions loaded within the resin beads by shaking with 250 mL of a binary NaCl–NaOH (1 M of each) solution under the same conditions as in the previous step. The solution was decanted and discarded likewise. The resin beads were then washed with DI water more than 10 times to remove all residual binary solution. The clean resins were finally dried in an oven set at 40 °C overnight for 16 h. Hence, the hybrid chelating ion-exchange metal oxide resins (HLIX-Zr) were produced for the purpose of this study.

2.3 Characterization of synthesized resins

Physical characterization of the synthesized resins was carried out on both the host and hybrid resins. The crystallinity was studied using XRD model Rigaku Smartlab X-ray Diffractometer at room temperature using Cu-Kα radiation ($\lambda = 0.154059$ nm) operated at 45 kV and 200 mA in a 2θ range of 5°–90° and speed 2° min^{-1}. The qualitative qualities of the dispersed nanoparticles were studied using HRSEM model JEOL JSM-7800F Field Emission Scanning Electron Microscope (FESEM) coupled with Thermo Scientific Ultradry EDS detector. Functional groups on the adsorbents' surfaces were investigated using Fourier transform infrared model PerkinElmer FTIR spectrometer Frontier (spectrum 100 spectrometer) by ATR method in the range of 400–4000 cm^{-1} at a resolution of 4 cm^{-1}.

2.4 Adsorption studies

Adsorption experiments were carried out using the batch equilibrium technique. Synthetic solution containing about 50 mg/L of each of Al(III), Fe(II) and Mn(II), the main metal constituents of AMD, was prepared in the presence of about 3000 mg/L SO_4^{2-} and used to model the adsorption efficiency of the synthesized nanosorbents. The salts that were used to prepare the ternary synthetic solution were supplied as $Al_2(SO)_4$ hydrate ($M_r = 242.2$ g/mol), $MnSO_4{\cdot}H_2O$ ($M_r = 98.08$ g/mol) and $FeSO_4{\cdot}7H_2O$

(M_r = 278.01 g/mol), and the weights for the salts used were 0.6356 g, 0.3000 g and 0.4976 g in 2 L, respectively. The batch tests were carried out in 100-mL Erlenmeyer flasks using 50 mL of synthetic solution in an orbital shaker set at 200 rpm, at 25 °C. Each flask was covered with parafilm to avoid evaporation during the adsorption process. A fixed amount of adsorbent (20 mg) at different time intervals (5, 10, 20, 30, 60, 180, 360 min) was used to study the effect of contact time on Al(III) ions' adsorption. The effect of adsorbent dosage (0–12 g/L) for the predetermined times on adsorption efficiency was conducted. The effect of initial pH (1.5–3.5 and 10.0–11.5) on adsorption of Al(III) ions was investigated at predetermined time and resin dosage. Al(III) precipitates around pH 4 and redissolves above pH 8; thus, no pH study can be conducted in this pH range for the Al(III). Kinetics and isotherm modelling was carried out using the adsorption data in the pH ranges where Al(III) is dissolved. Regeneration of the loaded hybrid resin was carried out using a NaCl–NaOH binary solution (3% w/v of each salt). The metal-loaded hybrid resin was washed with DI water to remove excess synthetic solution before 50 mL of regenerant solution was added. The flask was then shaken in the same conditions as the adsorption process. The amounts of metal ions in the solutions were estimated using Agilent Technologies 700 Series ICP-OES.

2.5 Application to environmental sample

The best performing hybrid nanosorbent was finally tested on environmental AMD, obtained from a defunct gold mine located in the western part of Gauteng Province, South Africa, for the removal of 10 selected metals (Al, Cr, Mn, Fe, Ni, Co, Cu, Zn, Pb and Cd). All experiments were carried out in triplicate, and the average result was reported. Blanks were also run together with the samples to establish the effect the glassware had on the adsorption of the metal ions.

2.6 Data analysis

The experimental concentration of metal adsorbed on the adsorbent was expressed as q_e (mg/g), which is calculated using Eq. 1:

$$q_e = \frac{V(C_o - C_e)}{m} \tag{1}$$

where C_o and C_e are the initial and final concentration of the metal ion in solution (mg/L), respectively, V is the volume of solution used (L) and m is the mass of adsorbent (g) that was used. In this study, the adsorption performance was also expressed as percentage using Eq. 2:

$$\%\text{Al(III)removal} = \frac{(C_o - C_e)}{C_o} \times 100 \tag{2}$$

where C_o and C_e are the same quantities as described for Eq. 1 [42].

3 Modelling of adsorption data

3.1 Kinetics models

The pseudo-first-order, pseudo-second-order and intraparticle diffusion models were used to study the kinetics of adsorption of Al(III) onto the HZO hybrids. The rate constant of the pseudo-first-order model is given by Eq. 3:

$$\ln(q_e - q_t) = \ln q_e - K_1 t \tag{3}$$

where q_e and q_t are the amount of Al(III) adsorbed in mg/g resin at equilibrium and at time t (min), respectively. K_1 is the pseudo-first-order rate constant for adsorption in (min^{-1}). Values of K_1 were calculated from the plots of $\ln(q_e - q_t)$ versus t for different time intervals. The pseudo-second-order kinetics model is given in Eq. 4:

$$\frac{t}{q_t} = \frac{1}{K_2 q_e^2} + \frac{1}{q_e} t \tag{4}$$

where q_t (mg/g) is the amount of analyte adsorbed at time t (min), q_e (mg/g) is the amount of analyte adsorbed at equilibrium and K_2 is the equilibrium rate constant for the pseudo-second-order sorption in g/mg min. The intraparticle diffusion model is expressed using Eq. 5:

$$q_t = K_i t^{\frac{1}{2}} + C \tag{5}$$

where q_t is the concentration of the analyte on the adsorbent surface in mg/g at time, t (min), K_i is the intraparticle rate constant in mg/g $\text{min}^{1/2}$ and C is the intercept in mg/g.

3.2 Adsorption isotherm models

Two-parameter adsorption isotherm models: Freundlich, Langmuir and Temkin, were used to describe the relationship between the amount of Al(III) ions remaining in solution after the adsorption process and the amount deposited on the surfaces of an adsorbent. The Freundlich isotherm assumes that the adsorption sites on the adsorbent surface are heterogeneous and hence have different binding energy, and there exist interactions between the adsorbed particles leading to multilayer adsorption [11]. The linearized form of the Freundlich is given in Eq. 6:

$$\log q_e = \frac{1}{n}\log C_e + \log K_F \quad (6)$$

The data conform to the Freundlich isotherm if log C_e plotted against log q_e yields a straight line.

The Langmuir isotherm assumes that the sites on the adsorbent surface are homogeneous with equal binding energy; there are no interactions between adsorbed species resulting in a monolayer adsorption. There are several linearized forms for this model, and the two that were used in this work are expressed in Eqs. 7 and 8:

$$\text{Langmuir type 1}: \frac{C_e}{q_e} = \frac{C_e}{q_{\max}} + \frac{1}{q_{\max}K_L} \quad (7)$$

$$\text{Langmuir type 4}: \frac{q_e}{C_e} = K_L q_{\max} - K_L q_e \quad (8)$$

where C_e is the concentration of the analyte remaining in solution (mg/L), q_e is the concentration of the analyte adsorbed (mg/g), q_{max} is the Langmuir constant related to adsorption capacity (mg/g) and K_L is the Langmuir constant related to energy of adsorption (L/mg). The linear plot for type 1 is obtained by plotting C_e versus $\frac{C_e}{q_e}$, and for type 4, q_e is plotted against $\frac{q_e}{C_e}$.

The Temkin isotherm, like the Freundlich model, is also used to describe adsorption on heterogeneous surfaces. The difference is in that the Temkin model assumes that the energy of adsorption decreases linearly with increase of coverage due to adsorbate–adsorbate interactions. The linearized Temkin model is described by Eq. 9:

$$q_e = \frac{RT}{b}\ln K_T + \frac{RT}{b}\ln C_e \quad (9)$$

where q_e and C_e are the concentration of the analyte on the solid phase (mg/g) and that remaining in the liquid phase (mg/L), respectively. K_T (L/g) and $\frac{RT}{b}$(dimensionless) are the Temkin constants.

The coefficient of determination (R^2) and the error function, nonlinear Chi-square statistic (χ^2), were used to determine the goodness of fit of the experimental data to the kinetics and isotherm models. A model that best describes an adsorption process gives the highest coefficient of determination (closest to 1) and the least Chi-square value. The Chi-square error function is calculated using Eq. 10 [42]:

$$\chi^2 = \sum \frac{(q_e \text{ experimental} - q_e \text{ calculated})^2}{q_e \text{ calculated}} \quad (10)$$

4 Results and discussion

4.1 Characterization of nanocomposites

A bead from each of the five hybrid HZO resins was dissected, and the cross-sectional area was scanned using the SEM–EDX analytical technique. The results, presented in Fig. 1, revealed that Zr was successfully incorporated within all the host resins.

It was never anticipated that the nanoparticles would affect the surface groups of the host resins as there is no chemical bond between the two after finalization of the synthetic procedure. The FTIR spectra in Fig. 2a show that indeed the incorporation of the HZO into the host resins beads did not tamper with the polymer surface functional groups. This is an intended outcome because both the host resin and the dispersed Zr oxide nanoparticles should complement each other in the adsorption process. The host resin is envisaged to enhance metal ion permeation, by the Donnan membrane effect [12], concurrently concentrating the analyte within the resin beads for effective adsorption by the dispersed Zr oxide nanoparticles. The broad band at 3300 cm^{-1} and peaks at 1600 cm^{-1} are due to O–H vibrational stretching and bending, respectively. The two P–O stretching phosphonate groups of the host and its hybrid were observed at 1100 and 950 cm^{-1}. In another study, in different media, the phosphonate P–O stretching at 1016 and 966 cm^{-1} has been reported [5]. The peaks at about 745.7 and 524.3 cm^{-1} are attributed to the Zr–O bond of the dispersed hydrated Zr oxide nanoparticles for the hybrid adsorbents [27]. The XRD spectra for the hybrid nanosorbents are illustrated in Fig. 2b. The broad peak with poor resolution observed at $2\theta = 20°$ for HZO-4195 and HZO-214 may be attributed to the amorphous phase of $Zr(OH)_4$. Similar peaks have been reported previously by Kobayashi et al. [26]. Hence, all the hybrid HZO nanocomposites are amorphous as shown by the absence of peaks in their spectra. This is a desirable feature for adsorbents because they need to have as much surface area as possible to achieve maximum adsorption sites for enhanced adsorption efficiencies.

4.2 Effect of contact time on Al^{3+} adsorption

The effect of time on the adsorption of Al(III) from a synthetic solution of pH 1.8 is investigated and reported in Fig. 3. The adsorption was very rapid on hybrid HZO-260 in the first 30 min and then gradually slowed down for the rest of the contact time. For HZO-207 and HZO-4195, the adsorption was so fast that it completed within

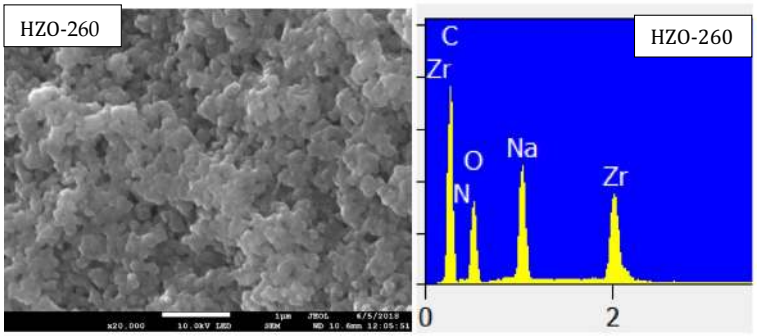

Element	Weight %
C	53.9
N	5.6
O	16.2
Na	11.1
Zr	13.2

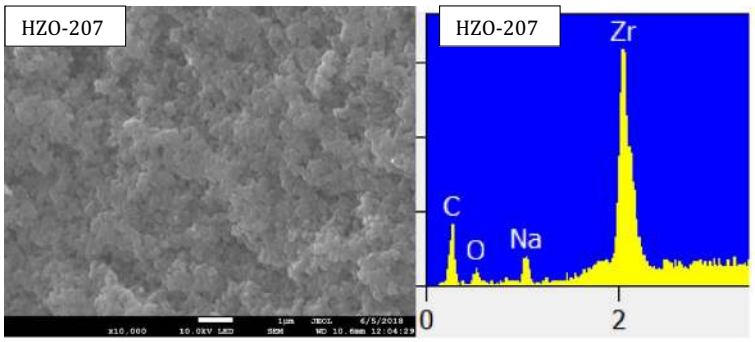

Element	Weight %
C	27.2
O	4.3
Na	2.4
Zr	66.2

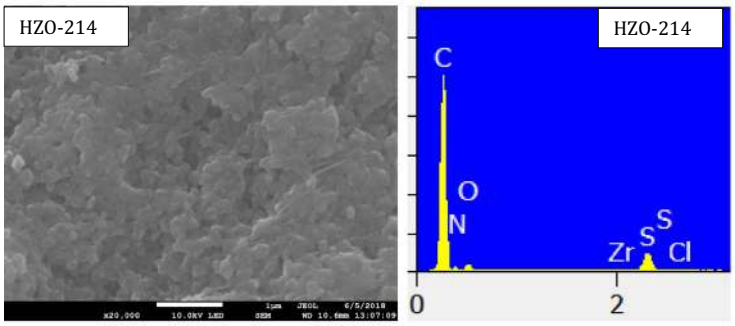

Element	Weight %
C	67.8
N	19.4
O	3.6
S	7.7
Cl	0.6
Zr	0.9

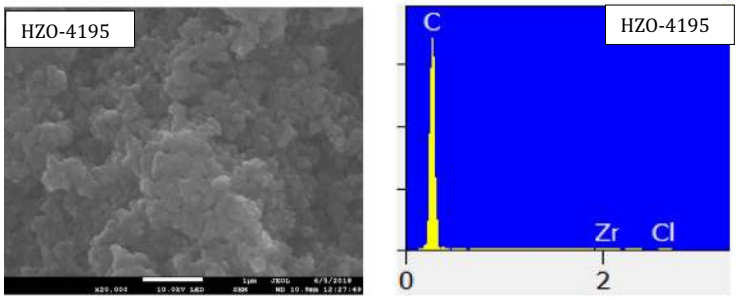

Element	Weight %
C	97.8
Cl	1.1
Zr	1.2

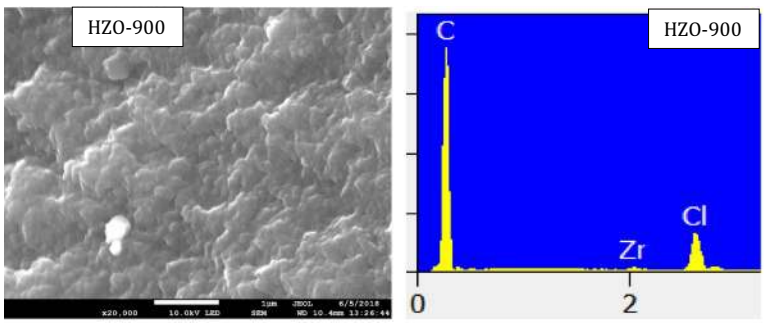

Element	Weight %
C	84.2
Cl	14.9
Zr	0.9

Fig. 1 SEM images and EDX spectra for the cross-sectional surface of hybrid HZO resins beads

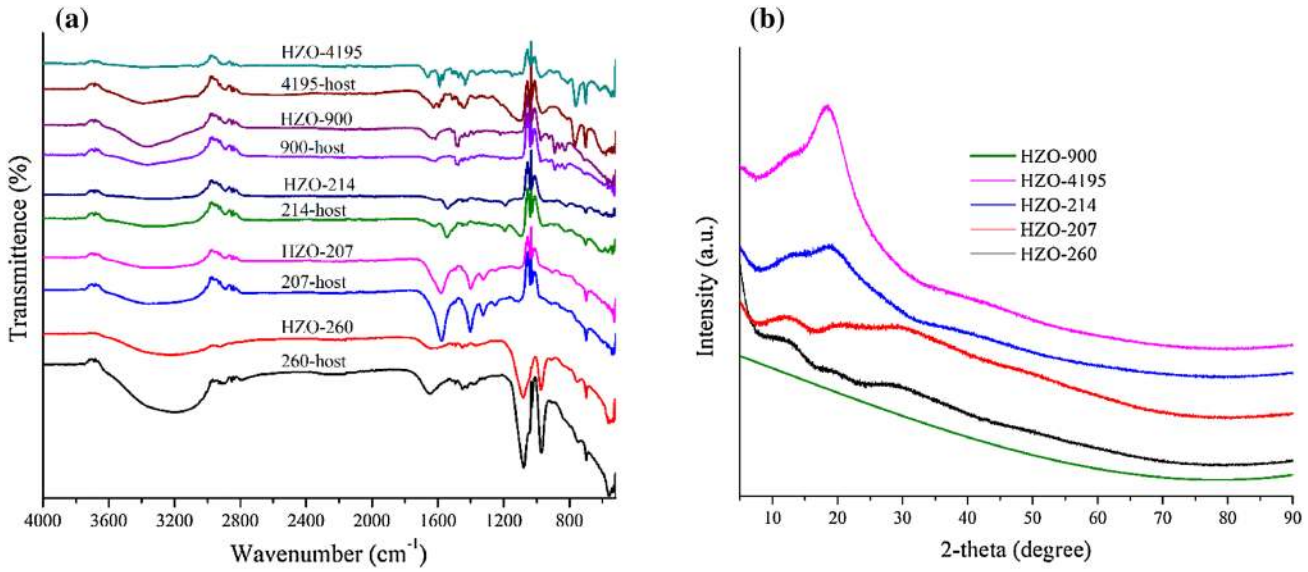

Fig. 2 **a** FTIR spectra of the host and the hybrid HZO resins, **b** powder XRD spectra of the hybrid HZO resins

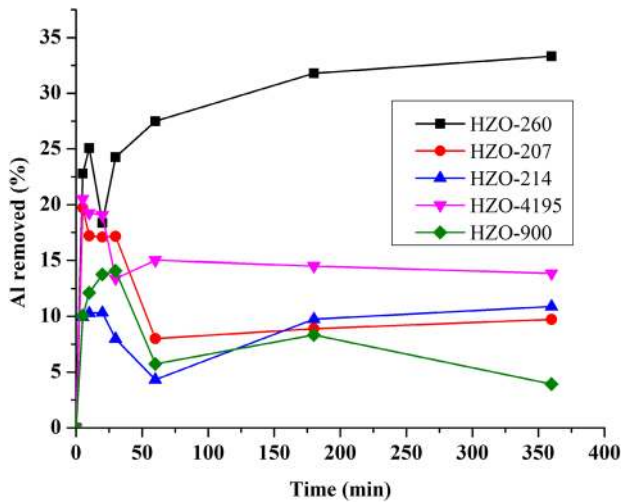

Fig. 3 Percentage Al(III) removed as a function of time in ternary Al–Fe–Mn solution; (0.02 g adsorbent; 50 mL synthetic solution; solution pH = 1.8; concentration of metals 50 mg/L for each; shaken at 25 °C; agitation speed 200 rpm)

5 min; thereafter, desorption was observed. HZO-207 recorded the most desorption (60%) at 60-min contact time; thereafter, adsorption occurred again but at a very slow rate. On the other hand, HZO-4195 desorbed only 25% of the adsorbed Al(III) at 60-min contact time and the desorption slowly proceeded for the rest of the contact time. Hybrid HZO-214 adsorbed rapidly in the first 20 min; thereafter, it released 60% of the Al(III) back into solution up to 60 min contact time. The nanocomposite then showed some very slow adsorption for the rest of the time allowed. The similarity in the adsorption rate pattern of HZO-207 and HZO-214 may be attributed to that their hosts are both weakly acidic ion-exchange chelating resins with one cation-exchange site, though on different functional groups. The readsorption might have been facilitated by electrostatic attractions between the fixed negative charges in the ion-exchange sites of the host resins and the Al cations in solution. The observed gradual readsorption of Al may be attributed to that after desorption, the Al(III) competes with the coexisting Fe(II) and Mn(II) ions for the created vacant sites on the adsorbent surface, but the adsorption of Al(III) is favourable owing to its higher ionic charge than the other two types of cations. Hybrid HZO-900 adsorbed rapidly in the first 10 min, then the rate depreciated up to 30 min of contact, and desorption of 57% was observed at 1 h of contact. Desorption proceeded slowly for the rest of the remaining time. This adsorption rate pattern of HZO-900 resembles that of HZO-4195 probably because both hybrids are hosted by anionic exchangers, a strong base and a weak base chelating resins, respectively. Anionic exchangers have fixed positive charges in their ion-exchange sites which strongly repel the highly charged Al cations than the coexisting Fe(II) and Mn(II) ions leading to difficult contact with the dispersed HZO for readsorption to occur. Hybrid HZO-260 exhibited the highest adsorption rate within the first 30 min, and thereafter, the adsorption was slow for the rest of the remaining time. This nanocomposite bound the Al(III) strongly because it did not release the adsorbed metal like the other nanocomposites.

Kinetics models are used to predict how the nature of the adsorbent and the adsorbate influences the rate at

which an analyte is removed from solution onto the surfaces of an adsorbent. This is paramount information when designing treatment plants. Batch kinetic data were fitted to three kinetic models: pseudo-first-order, pseudo-second-order and intraparticle diffusion. The adsorption data fitted best in the pseudo-second-order kinetics model as depicted by the highest coefficient of determination ($R^2 > 0.9$) which was the closest to unity as compared to the pseudo-first-order and intraparticle diffusion models (Table 1). Hence, the adsorption of Al(III) on all the nanocomposite adsorbents under study can be best described by the pseudo-second-order kinetics. The Chi-square (χ^2) statistic values that are far smaller for the pseudo-second-order kinetics compared to those of the first-order kinetics model confirm the findings. Small Chi-square values indicate that there are very small differences between each experimental and calculated capacity for a particular adsorbent, and the contrary is true. The obtained results are in agreement with findings obtained by other workers on adsorption of both organic and inorganic species from solutions [11, 19].

4.3 Effect of adsorbent dosage

The effect of adsorbent dosage on Al(III) removal from solution by the various nanocomposites is illustrated in Fig. 4. The amount of Al(III) ions removed from solution increased with increasing HZO-260 dosage to complete removal (100%) at dosage 8 g/L. This result is expected because the added adsorbent availed more fresh adsorption sites for the Al(III) uptake. In as much as the removal efficiency increased with dosage, the capacity of the adsorbent decreased with increasing adsorbent dosage. This result may be attributed to the low Al(III) concentration that was left in the solution such that the additional adsorbent fell short of Al(III) to adsorb. The overlapping of the resin beads due to overcrowding which caused some adsorption sites not to be accessible to the solution for Al(III) uptake leading to lower mass analyte adsorbed per gram resin may also be another factor. All the other hybrid nanosorbents exhibited unfavourable Al(III) adsorption (< 45%) in the acidic solution (pH 1.8). It may be presumed that the nanosorbents are not suitable for metal removal in acidic media and hence should be trialed in alkaline solutions.

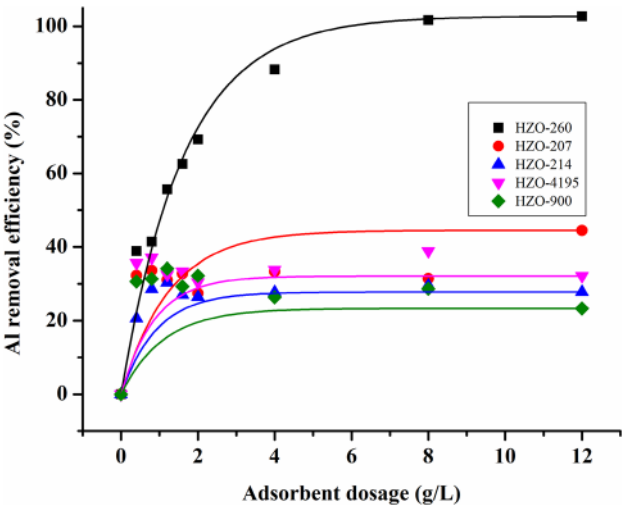

Fig. 4 Percentage Al(III) removed by the nanosorbents at varying dosage 0–12 g/L (50 mL synthetic Al–Fe–Mn solution; pH 1.8; shaken at 25 °C; agitation speed 200 rpm)

The equilibrium isotherms are critical data to provide insight on the mechanism of metal ions adsorption. In this work, the isotherm study was carried out using two-parameter models, namely Langmuir, Freundlich and Temkin (Table 2). The Chi-square statistic (χ^2) values show that the HZO-260 adsorption best fitted in the Freundlich model (depicted by lower value), while all the other adsorbents under study followed the Langmuir model. The adsorption of Al(III) on the HZO-260 nanosorbent best fitted to the Freundlich model ($R^2 = 0.9001$) with $n = 1.9019$ which indicated a favourable sorption process because $1 < n < 10$ [13]. According to Dlamini et al. [15], when $n > 1$ the adsorption process is predominantly governed by physisorption. Therefore, the adsorption of Al(III) onto the HZO-260 surfaces occurred through physical attraction of unlike charges although Tran et al. [42] argues that the Freundlich model fails to describe the saturation behaviour of an adsorbant. The favourable adsorption results were confirmed by the findings on the effect of initial solution pH where 100% Al(III) adsorption on HZO-260 was achieved

Table 1 Kinetics model parameters for Al^{3+} adsorption on HZO hybrids at solution pH 1.8

Hybrid nanosorbent	Pseudo-second-order			Pseudo-first-order			Intraparticle	
	K_{2p}	χ^2	R^2	K_{1p}	χ^2	R^2	K_{int}	R^2
HZO-260	0.0034	0.017	0.9986	0.0085	37.300	0.7309	−0.3357	0.8807
HZO-207	−0.0411	10.991	0.9947	−0.0035	66.432	0.1748	−0.7387	0.9941
HZO-214	0.0044	0.004	0.9397	0.0021	78.627	0.0632	0.1362	0.5807
HZO-4195	−0.0232	3.342	0.9996	−0.0025	93.086	0.0850	−0.6665	0.9020
HZO-900	−0.0126	0.951	0.9383	−0.0042	85.018	0.1589	1.2843	0.8889

Table 2 Freundlich, Langmuir and Temkin isotherm constants for the adsorption of Al^{3+} on HZO nanocomposites

HZO	Freundlich				Langmuir					Temkin	
	K_F	χ^2	n	R^2	K_L	Q_{max}	χ^2	R_L	R^2	K_T	R^2
260	4.9000	9.9679	1.9019	0.9001	0.6835	28.4090	29.839	0.0276	0.6867	1.4080	0.6115
207	8.34×10^{-9}	68.146	0.1698	0.1797	−0.0296	−0.0169	46.398	1.9220	0.9994	0.0423	0.0502
214	4.83×10^{-18}	42.111	0.0861	0.1798	−0.0259	−0.4324	35.303	1.4175	0.9932	0.0297	0.3521
4195	9.13×10^{5}	60.062	−0.2993	0.0150	−0.0313	−0.2268	16.205	2.2972	0.9994	0.0261	0.0660
900	3.64×10^{31}	41.486	−0.0503	0.5884	−0.0290	−0.0137	33.821	1.8172	0.9994	0.0258	0.2367

in acidic pH (Fig. 5a). The high efficiency of HZO-260 in acidic pH may be attributed to the host resin which has two cation-exchange sites and therefore exerts stronger Donnan membrane effect on the Al cations in solution allowing easy accessibility onto the dispersed HZO particles in the inner surfaces of the porous bead. Secondly, the host resin has a phosphonate head; the P is also a strong ligand, in addition to the O atoms, which chelates with the Al cations in solution.

All the other nanosorbents' adsorption processes showed best agreement with the Langmuir model ($R^2 > 0.99$). This result implies that the adsorption sites on each adsorbent surface have equal energy (homogeneous) and there were no interactions between adsorbed species resulting in a single layer of the adsorbed metals. However, the negative values of K_L give negative values of q_{msx} which implies that the Langmuir model is inadequate for explaining the adsorption processes of these nanocomposites [1, 2]. This finding is reinforced by that the four nanocomposite adsorbents had the Langmuir model separation factor $R_L > 1$, which implies that the adsorption of Al(III) on their surfaces was not favourable; adsorption is favourable in the range $0 < R_L < 1$. This result concurs with the findings on the effect of pH which showed low removal efficiencies for these hybrid adsorbents in acidic conditions (Fig. 5b–e). Moreover, the big Chi-square values show that the difference between the experimental and calculated capacity using the model is significant, confirming the inadequacy of the model to describe the adsorption processes regardless of being the model of best fit as per the coefficient of determination ($R^2 > 0.99$).

4.4 Effect of pH on the pattern of adsorption

The pH is the master parameter in the adsorption of metals from solutions. Figure 5a shows that hybrid HZO-260 removed all (100%) of the Al(III) in acidic conditions and adsorption was unfavourable in alkaline conditions. The preferred solution pH for efficient and sufficient use of the HZO-260 adsorbent is 2.0–2.4 because the final solution pH (6.6–7.5) is within pH 6.5–8.5, the drinking water guideline by the United States Environmental Protection Agency (USEPA) [43]. Thus, this nanocomposite is best suited for AMD remediation. HZO-207 (Fig. 5b) adsorbed Al(III) (85%) the best at alkaline pH (10.2) achieving a final solution pH of 8.1 which is within the drinking water guideline. This adsorbent may be suitable for the recovery of metals from alkaline solutions though this may be a very difficult process to control because at pH 11 desorption is favourable. HZO-214 adsorbed 100% Al(III) at pH 11.3 yielding a final solution pH of 7.66 that meets the drinking water guideline as shown in Fig. 5c. Similarly, the use of this adsorbent would pose a great challenge because at pH 10 metal adsorption is very unfavourable and the same is applicable at pH around 12. These two conditions would make the use of this hybrid material a very difficult process to control because of the very narrow pH operation range. Therefore, it is not cost-effective to adsorb Al(III) in alkaline conditions. It should be noted that the adsorption of Al(III) was not considered in the pH range of 4.5–9, where Al(III) precipitates as $Al(OH)_3$. Above pH 9, the $Al(OH)_3$ dissolves and Al(III) ions are released into the solution.

HZO-260, HZO-207 and HZO-214 are hosted by weak acid chelating resins of functional groups, methylaminophosphonate, iminodiacetate and thiourea, respectively, as mentioned earlier. All three nanocomposites can be used for Al(III) remediation at specific pH conditions. The pH at the point of zero charge (pH_{pzc}) for the adsorbents was estimated by making plots of the difference of pH_{final} from $pH_{initial}$ versus $pH_{initial}$. The adsorbent surface charge is positive below pH_{pzc} and negative above this critical point. The estimated pH_{pzc} for the nanocomposites is illustrated in Table 3. The pH_{pzc} for HZO-260 was 10.8, implying that the adsorbent performed best on a positive surface because it achieved 100% Al(III) removal in acidic pH. As mentioned earlier, Al mainly exists as a free Al^{3+} and $Al(SO_4)^+$ complex in acidic pH; hence, it may be concluded that the adsorption of the Al cations on HZO-260 occurred through chemical ion-exchange, either with the mobile cations of the host resin or with the abundant H^+ on the embedded Zr oxide nanoparticles surfaces. HZO-207 and HZO-214 both adsorbed best above their pH_{pzc}, 3.2 and 10.8, respectively, where their dominant surface charge is negative. This result is not surprising because

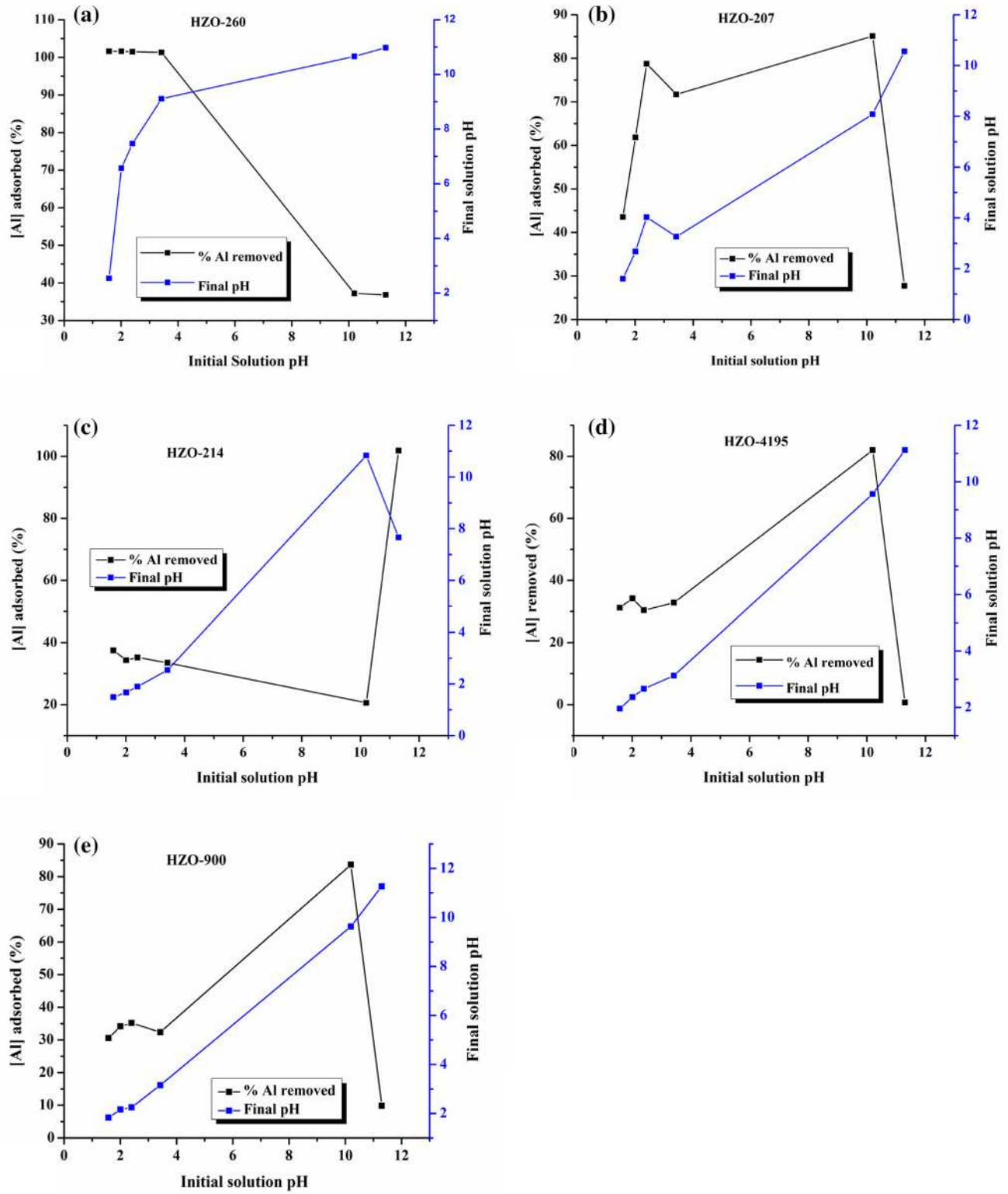

Fig. 5 Percentage Al(III) removed and final solution pH after adsorption using the hybrid nanocomposite adsorbents at initial pH range 1.5–3.5 and 10–11.5 at predetermined contact time and adsorbent dosage for each hybrid material (50 mL synthetic Al–Fe–Mn solution; shaken at 25 °C; agitation speed 200 rpm)

Table 3 Summary of the effect of pH observations for the hybrid adsorbents under study

Hybrid	pH initial	Estimated pzc	Adsorption efficiency (%)	Final solution pH
HZO-260	1.6, 2.0, 2.4, 3.4	10.8	100	2.5, 6.6, 7.5, 9.1
HZO-207	10.2	3.2	85	8.1
HZO-214	11.3	10.8	100	7.7
HZO-4195	10.2	2.5	82	9.6
HZO-900	10.2	2.2	84	11.3

both adsorbents performed best at alkaline pH (10.2 and 11.3) where Al(III) exists as a negative complex, $Al(OH)_4^-$, in solution; hence, the adsorption may have occurred through chemical anion-exchange with the negative surface groups of the adsorbent. Secondly, OH^- has a high sorption affinity for metal oxides [31] and hence the favourable adsorption of the $Al(OH)_4^-$ complex onto the Zr oxide nanoparticles which may be achieved through ligand exchange.

Hybrid HZO-4195 and HZO-900, as shown in Fig. 5d and e, respectively, adsorbed Al(III) (82% and 84%, respectively) best at alkaline conditions of pH 10.2, but the final solution pH (9.6 and 11.3) failed to meet the USEPA drinking water guideline. The host resins for these two hybrid materials are a weak base chelating resin (bis-picolylamine) and a strong base anion exchanger, respectively; hence, they have fixed positive charges that exert Donnan membrane effect on the negative Al(III) complex, $Al(OH)_4^-$, in the alkaline medium. In light of the estimated pH_{pzc} (2.5 and 2.2) for the two adsorbents and the negative Al(III) complex in alkaline pH, the adsorption process must have happened through chemical ion-exchange with both the mobile anion of the host resin and the negative surface functional groups of the Zr oxide nanoparticles (ligand exchange). The slight difference in performance between these two hybrid materials may be attributed to the basic anionic strength of the host material. Nevertheless, both hybrid resins can be used to remove some metals in alkaline wastewater as part of a treatment train.

4.5 Regeneration studies

It is not sufficient to base the suitability of an adsorbent for application only on its high adsorption efficiency but its ease to be regenerated also plays a crucial role. A good adsorbent must be amenable to regeneration for reuse. Thus, desorption studies were carried out using only the HZO-260 adsorbent because it surpassed all the others in the metal removal efficiency in acidic synthetic water. Figure 6 shows that the hybrid adsorbent is not only a super adsorbent [99.67% Al(III)] but is also amenable to efficient regeneration for reuse using a NaCl–NaOH binary solution. The regenerant effluent contained 92.22% of the Al(III) that

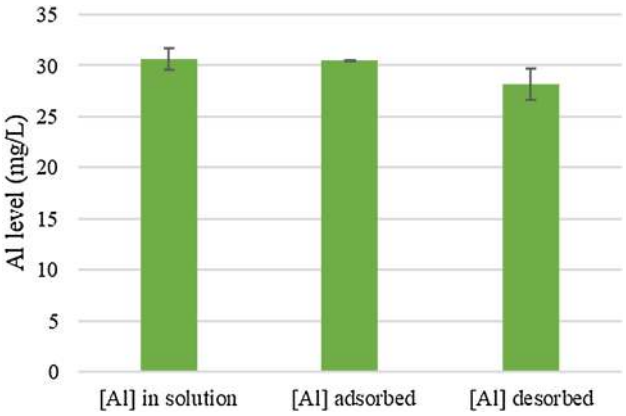

Fig. 6 Mean Al(III) level in test solution and that which was adsorbed and desorbed by hybrid HZO-260 nanosorbent (dosage 12 g/L; shaking speed 200 rpm; temperature 25 °C; 50 mL synthetic solution; time 360 min)

was adsorbed on the resin which concurs with the findings by Pan et al. [32] and Padungthon et al. [31]. The coexisting Fe(II) (98.99% adsorption) and Mn(II) (97.48% adsorption) were very low in the regenerant solution recording 0.59% and 0.01%, respectively. This result may be ascribed to that at the high pH (12.5), where the desorption was carried out, these two metal ions precipitate out of solution, and the precipitate was observed in the regenerant effluent in this study. The desorbed Al(III) and the precipitated Fe and Mn can be recovered from the regenerant effluent, by altering the pH or otherwise, as saleable products in a bid to protect the environment from secondary pollution. The revenue accrued from the sale of the recovered products would be used to finance the running costs of the process.

4.6 Application on environmental AMD

HZO-260 was chosen and tested on AMD obtained from a disuse gold mine in the western part of Gauteng, South Africa. The choice was based on that HZO-260 performed best in metals removal from synthetic water. The removal of Al(III), Fe(II) and Mn(II) from the synthetic solution of pH 1.8 corresponds to 99.67%, 98.99% and 97.48%,

Table 4 Mean metal levels (mg/L) in environmental AMD

Metal (M)	Al	Cd	Co	Cr	Cu	Fe	Mn	Ni	Pb	Zn
[M](mg/L)	836.62	0.64	15.83	1.79	4.63	412.27	105.09	32.91	0.65	36.40
SD	16.70	0.01	0.29	0.02	0.09	8.33	1.95	0.76	0.01	0.71

SD standard deviation

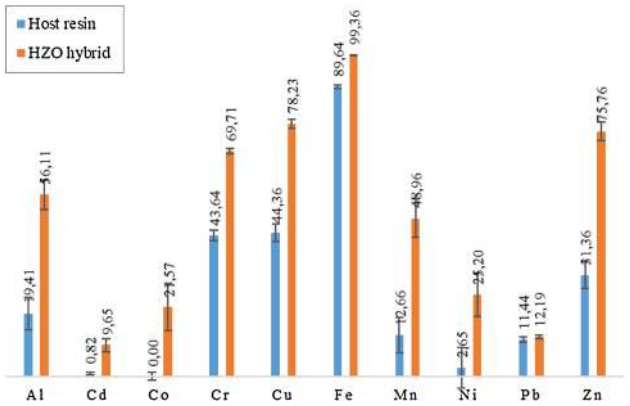

Fig. 7 Percentage metal removed from AMD by HZO-260 nanocomposite and its host resin (dosage 12 g/L; shaking speed 200 rpm; temperature 25 °C; 50 mL AMD; pH 2.46; time 360 min)

respectively. All the other hybrid adsorbents in this study removed Al(III) best (> 83%) in alkaline conditions of pH > 10 where the coexisting Fe(II) and Mn(II) ions had precipitated out of solution. Table 4 shows the selected metals (Al, Cr, Mn, Fe, Ni, Co, Cu, Zn, Pb and Cd) concentrations in the real AMD sample (pH 2.46) that was used to test the performance of the hybrid resin, while Fig. 7 shows the metal removal efficiency of both the hybrid resin and its host resin. The hybrid resin achieved higher metal removal efficiency than that of its host resin for all the metals investigated. The pH of the treated AMD was 3.3 and 3.0 for the HZO-260 nanosorbent and the host resin, respectively. The enhanced removal efficiency for the hybrid nanocomposite may be attributed to that both the host resin and the dispersed Zr oxide nanoparticles were involved in the metal adsorption process. The fixed negative charges on the host resin facilitated permeation of the metal cations through the Donnan membrane effect causing the analytes to access the Zr oxide nanoparticles dispersed within the pores of the resin beads for adsorption to occur. Some metal cations were adsorbed onto the active sites of the host resin. This result clearly has shown that incorporation of Zr into the host resin enhanced the metal removal efficiency from AMD. Therefore, the hybrid HZO-260 has a promising potential as an adsorbent for the remediation of AMD pollution.

5 Conclusion

Based on this study, incorporation of Zr oxide nanoparticles into the chelating resins was found very important. This is in terms of enhancing metal removal efficiency from AMD as well as improving the stability of the adsorbent in acidic media. Amongst the synthesized hybrid resins, HZO-260 was found the best in adsorption efficiency of metals at a lower pH ≤ 3.4. The other nanocomposites, HZO-207, HZO-214, HZO-4195 and HZO-900, can remove metals appreciably only in alkaline solutions, which is not cost-effective. Adsorption of Al(III) by HZO-260 from real AMD occurs through physisorption (chemical ion-exchange). Application of HZO-260 for metal removal from the environmental AMD sample revealed that removal of Mn(II) in acidic medium is possible. Furthermore, in order to apply HZO-260 in future for real AMD remediation, possible number of recycle and reuse, cost–benefit calculation and optimization of all parameters need to be addressed. Overall, from these results hybrid HZO-260 nanocomposite is a potential and promising candidate for future AMD pollution remediation.

Acknowledgements The authors are grateful for laboratory working space from the College of Agriculture and Environmental Sciences (CAES), use of ICP-OES from the Analytical Chemistry Department, use of XRD and HRSEM from the Physics Department and funding from the NanoWS Research Unit, all from UNISA Science Campus, Johannesburg, South Africa.

Compliance with ethical standards

Conflict of interest The author(s) declare that they have no competing interests.

References

1. Alsenani G (2013) Studies on adsorption of crystal violet dye from aqueous solution onto calligonum comosum leaf powder (CCLP). J Am Sci 9:30–35
2. Alshabanat M, Alsenani G, Almufarij R (2013) Removal of crystal violet dye from aqueous solutions onto date palm fiber by adsorption technique. J Chem. https://doi.org/10.1155/2013/210239
3. Azapagic A (2004) Developing a framework for sustainable development indicators for the mining and minerals industry.

J Clean Prod 12:639–662. https://doi.org/10.1016/S0959-6526(03)00075-1
4. Benner S, Blowes D, Gould WD, Herbert JRR, Ptacek CJ (1999) Geochemistry of a permeable reactive barrier for metals and acid mine drainage. Environ Sci Technol 33:2793–2799. https://doi.org/10.1021/es981040u
5. Bingol HB, Demir Duman F, Yagci Acar H, Yagci MB, Avci D (2018) Redox-responsive phosphonate- functionalized poly(β-amino ester) gels and cryogels. Eur Polym J 108:57–68. https://doi.org/10.1016/j.eurpolymj.2018.08.029
6. Bondy SC (2010) The neurotoxicity of environmental aluminum is still an issue. Neurotoxicology 31:575–581. https://doi.org/10.1016/j.neuro.2010.05.009
7. Chamier J, Wicht M, Cyster L, Ndindi NP (2015) Aluminium (Al) fractionation and speciation; getting closer to describing the factors influencing Al^{3+} in water impacted by acid mine drainage. Chemosphere 130:17–23. https://doi.org/10.1016/j.chemosphere.2015.01.026
8. Cho DW, Jeon BH, Jeong Y, Nam IH, Choi UK, Kumar R, Song H (2016) Synthesis of hydrous zirconium oxide-impregnated chitosan beads and their application for removal of fluoride and lead. Appl Surf Sci 372:13–19. https://doi.org/10.1016/j.apsusc.2016.03.068
9. Coelho P, Teixeira J, Gonçalves O (2011) Mining activities: health impacts. Encycl Environ Health. https://doi.org/10.1016/B978-0-444-52272-6.00488-8
10. Cravotta CA (2008) Dissolved metals and associated constituents in abandoned coal-mine discharges, Pennsylvania, USA. Part 2: geochemical controls on constituent concentrations. Appl Geochem 23:203–226. https://doi.org/10.1016/j.apgeochem.2007.10.003
11. Crini G, Peindy HN, Gimbert F, Robert C (2007) Removal of C. I. Basic Green 4 (Malachite Green) from aqueous solutions by adsorption using cyclodextrin-based adsorbent: kinetic and equilibrium studies. Sep Purif Technol 53:97–110. https://doi.org/10.1016/j.seppur.2006.06.018
12. Cumbal L, Greenleaf J, Leun D, SenGupta AK (2003) Polymer supported inorganic nanoparticles: characterization and environmental applications. React Funct Polym 54:167–180. https://doi.org/10.1016/S1381-5148(02)00192-X
13. Dada AO, Olalekan AP, Olatunya AM, Dada O (2012) Langmuir, Freundlich, Temkin and Dubinin–Radushkevich isotherms studies of equilibrium sorption of Zn(11) onto phosphoric acid modified rice husk. IOSR J Appl Chem 3:38–45. https://doi.org/10.9790/5736-0313845
14. Dlamini CL, Fadiran AO, Thwala JM (2013) A study of environmental assessment of acid mine drainage in Ngwenya, Swaziland. J Environ Prot 4:20–26. https://doi.org/10.4236/jep.2013.411B003
15. Dlamini DS, Mishra AK, Mamba BB (2012) Kinetic and equilibrium studies of the removal of Pb^{2+} from aqueous solutions using Na_2SO_4-EVA/Cloisite® 20A composite. Mater Chem Phys 133:369–375. https://doi.org/10.1016/j.matchemphys.2012.01.040
16. Durand JF (2012) The impact of gold mining on the Witwatersrand on the rivers and karst system of Gauteng and North West Province, South Africa. J Afr Earth Sci 68:24–43. https://doi.org/10.1016/j.jafrearsci.2012.03.013
17. Edwards M, Benjamin MM (1989) Regeneration and reuse of iron hydroxide adsorbents in treatment of metal-bearing wastes. J Water Pollut 61:481–490
18. Gray A, Vawda Y (2016) South African health review. In: South African health review 2016, Padarath A, King J, Mackie E, Casciola J (Eds) p 1–369
19. Ho YS, Mckay G, Wase DAJ (2000) Study of the sorption of divalent metal ions on to peat. Adsorpt Sci Technol 18:639–650. https://doi.org/10.1260/0263617001493693
20. Hua M, Jiang Y, Wu B, Pan B, Zhao X, Zhang Q (2013) Fabrication of a new hydrous Zr (IV) oxide-based nanocomposite for enhanced Pb(II) and Cd (II) removal from waters. Appl Mater Interfaces 5:12135–12142
21. Humby T (2013) Environmental justice and human rights on the mining wastelands of the Witwatersrand gold fields environmental justice and human rights on the mining wastelands of the Witwatersrand gold fields du tudor shaft informal. Rev Gen Droit 43:67–112. https://doi.org/10.7202/1021211ar
22. Jaishankar M, Tseten T, Anbalagan N, Mathew BB, Beeregowda KN (2014) Toxicity, mechanism and health effects of some heavy metals. Interdiscip Toxicol 7:60–72. https://doi.org/10.2478/intox-2014-0009
23. Jennings SR, Blicker S, Neuman P, Dennis R (2008) Acid mine drainage and effects on fish health and ecology: a review. Reclam Res Gr 1:1–26
24. Johnson DB, Hallberg KB (2005) Acid mine drainage remediation options: a review. Sci Total Environ 338:3–14. https://doi.org/10.1016/j.scitotenv.2004.09.002
25. Kefeni KK, Msagati TAM, Mamba BB (2017) Acid mine drainage: prevention, treatment options, and resource recovery: a review. J Clean Prod 151:475–493. https://doi.org/10.1016/j.jclepro.2017.03.082
26. Kobayashi T, Sasaki T, Takagi I, Moriyama H (2007) Solubility of zirconium (IV) hydrous oxides. J Nucl Sci Technol 44:90–94
27. Mahmoud ME, Abdou AEH, Sobhy ME (2017) Engineered nanozirconium oxide-crosslinked- nanolayer of carboxymethyl cellulose for speciation and adsorptive removal of Cr(III) and Cr(VI). Powder Technol 321:444–453. https://doi.org/10.1016/j.powtec.2017.08.041
28. Martinez M, Leyton Y, Cisternas LA, Riquelme C, Serena L (2018) Metal removal from acid waters by an endemic microalga from the Atacama Desert for water recovery. Minerals 8(378):1–14. https://doi.org/10.20944/preprints201808.0008.v1
29. Moodley I, Sheridan CM, Kappelmeyer U, Akcil A (2017) Environmentally sustainable acid mine drainage remediation: research developments with a focus on waste/by-products. Miner Eng 126:207–220. https://doi.org/10.1016/j.mineng.2017.08.008
30. Munnik V (2010) The social and environmental consequences of coal mining in South Africa. Environ Monit, Gr, p 24
31. Padungthon S, German M, Wiriyathamcharoen S, SenGupta AK (2015) Polymeric anion exchanger supported hydrated Zr(IV) oxide nanoparticles: a reusable hybrid sorbent for selective trace arsenic removal. React Funct Polym 93:84–94. https://doi.org/10.1016/j.reactfunctpolym.2015.06.002
32. Pan B, Li Z, Zhang Y, Xu J, Chen L, Dong H, Zhang W (2014) Acid and organic resistant nano- hydrated zirconium oxide (HZO)/poly-styrene hybrid adsorbent for arsenic removal from water. Chem Eng J 248:290–296. https://doi.org/10.1016/j.cej.2014.02.093
33. Pan B, Wu J, Pan B, Lv L, Zhang W, Xiao L, Wang X, Tao X, Zheng S (2009) Development of polymer- based nanosized hydrated ferric oxides (HFOs) for enhanced phosphate removal from waste effluents. Water Res 43:4421–4429. https://doi.org/10.1016/j.watres.2009.06.055
34. Pandey N, Shukla SK, Singh NB (2017) Water purification by polymer nanocomposites: an overview. Nanocomposites 0324:1–20. https://doi.org/10.1080/20550324.2017.1329983
35. Poléo ABS, Østbye K, Øxnevad SA, Andersen RA, Heibo E, Vøllestad LA (1997) Toxicity of acid aluminium-rich water to seven freshwater fish species: a comparative laboratory study. Environ Pollut 96:129–139. https://doi.org/10.1016/S0269-7491(97)00033-X

36. Povar I, Spinu O (2014) The role of hydroxy aluminium sulfate minerals in controlling Al^{3+} concentration and speciation in acidic soils. Cent Eur J Chem 12:877–885. https://doi.org/10.2478/s11532-014-0540-4
37. Rosseland BO, Eldhuset TD, Staurnes M (1990) Environmental effects of aluminium. Environ Geochem Health 12:17–27. https://doi.org/10.1007/BF01734045
38. Samiey B, Cheng C, Wu J (2014) Organic-inorganic hybrid polymers as adsorbents for removal of heavy metal ions from solutions: a review. Materials (Basel) 7:673–726. https://doi.org/10.3390/ma7020673
39. Sarkar S, Chatterjee PK, Cumbal LH, SenGupta AK (2011) Hybrid ion exchanger supported nanocomposites: sorption and sensing for environmental applications. Chem Eng J 166:923–931. https://doi.org/10.1016/j.cej.2010.11.075
40. Shen L, Muduli K, Barve A (2015) Developing a sustainable development framework in the context of mining industries: aHP approach. Resour Policy 46:15–26. https://doi.org/10.1016/j.resourpol.2013.10.006
41. Sun J, Zhou S, Hou P, Yang Y, Weng J, Li X, Li M (2006) Synthesis and characterization of biocompatible Fe_3O_4 nanoparticles. J Biomed Mater Res, Part A. https://doi.org/10.1002/jbm.a.30909
42. Tran HN, You SJ, Hosseini-Bandegharaei A, Chao HP (2017) Mistakes and inconsistencies regarding adsorption of contaminants from aqueous solutions: a critical review. Water Res 120:88–116. https://doi.org/10.1016/j.watres.2017.04.014
43. USEPA (2009) National primary/secondary and drinking water regulations. USEPA, Washington, D.C.
44. Zhang Q, Du Q, Hua M, Jiao T, Gao F, Pan B (2013) Sorption enhancement of lead ions from water by surface charged polystyrene-supported nano-zirconium oxide composites. Environ Sci Technol 47:6536–6544. https://doi.org/10.1021/es400919t
45. Zhang Q, Jiang P, Pan B, Zhang W, Lv L (2009) Impregnating zirconium phosphate onto porous polymers for lead removal from waters: effect of nanosized particles and polymer chemistry. Ind Eng Chem Res 48:4495–4499. https://doi.org/10.1021/ie8016847
46. Zheng H, Gao X, Song L, Guo H (2011) Preconcentration of trace aluminum (III) ion using a nanometer-sized TiO_2-silica composite modified with 4-aminophenylarsonic acid, and its determination by ICP-OES. Microchim Acta 175:225–231. https://doi.org/10.1007/s00604-011-0667-3